ACS OMEGA

http://pubs.acs.org/journal/acsodf

Article

Differences in Deterioration Behaviors of $Cu/ZnO/Al_2O_3$ Catalysts with Different Cu Contents toward Hydrogenation of CO and CO_2

Tanutporn Kamsuwan, Adisak Guntida, Piyasan Praserthdam, and Bunjerd Jongsomjit*

Cite This: *ACS Omega* 2022, 7, 25783−25797

Read Online

ACCESS | Metrics & More | Article Recommendations | Supporting Information

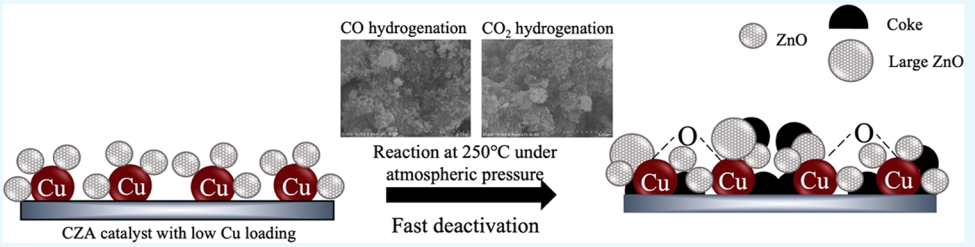

ABSTRACT: The deterioration behaviors of $Cu/ZnO/Al_2O_3$ (CZA) catalysts upon different Cu contents were elucidated. The fresh and spent catalysts after being used in CO and CO_2 hydrogenation at 250 °C under atmospheric pressure were properly characterized using various techniques including X-ray powder diffraction, X-ray photoelectron spectroscopy, and temperature-programmed reduction for the changes of metal sites, while the textural and chemical properties and carbon deposition on spent CZA catalysts were analyzed by N_2 physisorption, energy-dispersive X-ray spectroscopy, and temperature-programmed oxidation. During the hydrogenation reaction for both CO and CO_2, the unstable Cu^0 site on the spent CZA catalyst having a low Cu loading (sCZA-L) was oxidized to CuO and the aggregation of metal crystallite sites (Cu-ZnO and ZnO) was observed. Moreover, the amount of carbon deposition on sCZA-L (ca. >2%) is higher than the spent CZA catalyst having a high Cu loading (sCZA-H, ca. <0.5%). These phenomena led to a decrease in the surface area and the blockage of active sites. These findings can be determined on the catalytic deactivation and the obvious decrease in the catalytic activity of the CZA catalyst having a low Cu content (CZA-L, Cu:Zn = 0.8).

1. INTRODUCTION

The catalytic hydrogenation reactions of CO and CO_2 in recent years received great attention and have become the most promising route in many chemical industries for commercial methanol synthesis, which is a highly valuable chemical product.[1,2] The commercial methanol synthesis is performed under 50−100 atm at 200−300 °C for both CO and CO_2 hydrogenation reactions.[3−5] In general, methanol is an industrial organic solvent commonly used in organic synthesis and is also employed in many fields such as the plastic industry, clean chemical processes (biodiesel, DME, and higher hydrocarbons), and methanol-to-olefin (MTO) processes.[6,7] For these reactions, copper (Cu)-based catalysts mostly prepared by a coprecipitation method have been extensively studied in the recent decade, especially the ternary $Cu/ZnO/Al_2O_3$ catalyst. It has been widely used as an industrial catalyst for methanol production. According to several literature studies, they suggested that the metal Cu species are commonly regarded as the main active sites for methanol production, although the Cu-rich molar ratio in Cu-based catalysts results in a drop in the catalytic lifetime by the behaviors of active metal sintering and metal agglomeration. The addition of ZnO can enhance the stability of Cu species by the creation of Cu-ZnO interfacial sites and support the activation of synergistic effect to facilitate methanol formation via formate intermediates.[8] Furthermore, Al_2O_3 promoters (promotional effect), which have a high surface area, disperse active Cu sites and adjust the reducibility of ZnO.[9,10] Therefore, $Cu/ZnO/Al_2O_3$ catalysts have been well-known as the catalyst for CO and CO_2 hydrogenation, and they are regularly used as a standard catalyst in the methanol production industry. They are considered to have high potential for catalytic activity because of their structural properties, proper metal active sites, metal dispersion, and neutral and basic functions. Moreover, $Cu/ZnO/Al_2O_3$ catalysts are easy to synthesize with low cost and high performance. These suggestions were also corroborated by many literature studies.[1,8,11−13] The catalytic activity of traditional $Cu/ZnO/Al_2O_3$ catalysts depends on many reasons including the effect of operating conditions (i.e., pressure and

Received: May 17, 2022
Accepted: July 4, 2022
Published: July 14, 2022

https://doi.org/10.1021/acsomega.2c03068
ACS Omega 2022, 7, 25783−25797

temperature) and properties of catalysts (i.e., copper crystallite size, copper surface, and metal dispersion). Additionally, the limit of catalytic activity has found that the traditional Cu/ZnO/Al_2O_3 exhibits a poor activity and low yield of methanol in long-term catalytic reactions because of its behaviors of catalytic deactivation such as active metal sintering, coking, and byproduct formation to deactivate the catalyst surface.[6,11] Therefore, from the viewpoint of catalytic deactivation, it is highly important to clarify and elucidate this problem to improve the catalytic activity and increase the yield of methanol production in the future.

Deactivation of solid catalysts is a main problem in the industrial catalytic processes, which directly results in the loss of catalytic activity and/or selectivity in long-term application. Several candidates that are causes for deactivation were identified. In the present investigation, the mechanism of heterogeneous catalytic deactivation can be commonly divided into many types: poisoning, fouling or coking, thermal degradation and/or sintering, phase transformation (i.e., vapor compound formation and/or leaching accompanied by transport from the catalyst surface or particle, and vapor−solid and/or solid−solid reactions), and attrition or crushing.[14−16] In the case of solid catalysts, there are three types of components, namely, active components, auxiliary agents, and carriers, depending on the functionality. Basically, the active components are very important for the catalytic performance of catalysts, so the change of active components by loss of active species (such as the blockage active species and catalyst sintering) will directly influence the catalytic activity for catalytic reaction processes. In all these recent reports, there are many literature studies that investigated the activity of $Cu/ZnO/Al_2O_3$ via CO and CO_2 hydrogenation to methanol, whereas there are only few reports that discuss in depth the mechanism of deactivation of $Cu/ZnO/Al_2O_3$ catalysts.[13,17,18] However, active metal (Cu crystallites) sintering, agglomeration of ZnO species, oxidation of surface metallic Cu, byproduct deposition, and carbon deposition over the active component are usually the significant key factors of $Cu/ZnO/Al_2O_3$ catalyst deactivation according to the report of Fichtl et al.[15] and Peláez et al.[19] that discussed the phenomenon of the mechanism of catalytic deactivation. Among the above investigations, it is generally agreed that all reasons result in the loss of interfacial sites between ZnO and Cu, which are considered as the active sites for methanol synthesis from CO and CO_2 hydrogenation.

In our previous work,[3] the effect of different copper (Cu) loadings of ternary $Cu/ZnO/AL_2O_3$ (CZA) catalysts for catalyst screening on the characteristics and catalytic properties in CO and CO_2 hydrogenation reactions under mild conditions was investigated. We found that CZA catalysts having a high Cu loading (CZA-H) have enhanced catalytic properties. Their properties resulted in high catalytic activity (high conversion of CO and CO_2) and catalytic performance. Moreover, the catalytic deactivation results (from TGA) indicated that CZA-L (low Cu loading) is more easily deactivated than CZA-H. According to these previous results, it is not enough to conclude the deactivation behaviors of CZA catalysts in both CO and CO_2 hydrogenation reactions. Therefore, elucidation of the deactivation behaviors could be further conducted to determine the catalytic behaviors regarding the deactivation of catalysts. Furthermore, this research also aims to elucidate the effect of Cu loading of spent CZA (sCZA) catalysts on the catalytic deactivation after being tested via CO and CO_2 hydrogenation reactions and to determine the changes in textural and chemical properties of catalysts upon use.

2. EXPERIMENTAL METHODS

2.1. Materials and Preparation. The chemicals used for preparation of the catalysts[3] were aluminum nitrate nonahydrate [$Al(NO_3)_3{\cdot}9H_2O \geq 98\%$, Sigma-Aldrich], zinc nitrate hexahydrate [$Zn(NO_3)_2{\cdot}6H_2O \approx 98\%$, Sigma-Aldrich], copper(II) nitrate hemi (pentahydrate) [$Cu(NO_3)_2{\cdot}2.5H_2O \approx 98\%$, Sigma-Aldrich], and sodium hydrogen carbonate ($NaHCO_3$, Sigma-Aldrich). Gases employed for the characterization and reaction study were N_2 (99.99%), H_2 (99.99%), He (99.99%), air zero balance nitrogen, 10% H_2 in Ar mixed gas, and 1% O_2 in He mixed gas, which were purchased from Linde (Thailand) Public Company Ltd.

The preparation procedure to synthesize the tertiary Cu/ZnO/Al_2O_3 (CZA) catalyst with different copper (Cu) loadings by the coprecipitation method was described in our previous report.[3] Two CZA catalysts with different Cu contents were prepared using $Al(NO_3)_3{\cdot}9H_2O$, $Zn(NO_3)_2{\cdot}6H_2O$, and $Cu(NO_3)_2{\cdot}2.5H_2O$ as precursors. All precursors with the desired amount were dissolved in DI water as a solvent in the solution mixed at 80 °C, and then $NaHCO_3$ was slowly dropped into the metal solution to adjust the pH of the solution until the pH was 7. The precipitate solution was stirred for 60 min, and after that, the resulting product in coprecipitation was dried and calcined at 350 °C for 3 h to obtain the CZA catalyst. The catalysts prepared by this procedure were designated as CZA-L and CZA-H, where L refers to a low amount of Cu loading (Cu:Zn = 0.8) and H refers to a high amount of Cu loading (Cu:Zn = 3.0), respectively.

The spent catalysts after reaction testing were used to describe the catalytic deactivation in this study. The activity of 0.1 g CZA catalysts (CZA-L and CZA-H) was tested via CO and CO_2 hydrogenation in a fix-bed microreactor (O.D. 12 mm, I.D. 10 mm, length 500 mm) as reported in our previous study.[3] The experimental setup for catalytic reaction evaluation is shown in the Supporting Information in Figure S1. Prior to testing, the CZA catalyst was treated in N_2 flow (40 mL/min) at 250 °C for 30 min to remove any humidity on the catalyst surface. The catalyst reducibility (copper oxide to copper metal) was performed in H_2 flow at 300 °C for 60 min before the catalytic tests. The reaction of CO and CO_2 hydrogenation was carried out at 250 °C with a time on stream of 300 min under atmospheric pressure with mixtures of $CO:H_2$ = 1:2 and $CO_2:H_2$ = 1:3. A gas chromatograph (GC) with multidetectors (thermal conductivity detector (TCD, Shincarbon column) and flame ionization detector (FID, Rtx-5 column)) was used to detect the gas product.

2.2. Catalyst Characterization of Spent CZA Catalysts. For the difference in characteristics of catalytic deactivation, different characterization techniques were employed. For analysis of the spent CZA catalyst, the CZA-L and CZA-H catalysts were taken after the CO and CO_2 hydrogenation for 300 min at 250 °C as also mentioned in our previous work.[3] All catalysts were stored in N_2 flow to cool down from reaction temperature to room temperature before the measurement of all samples. After that, the spent catalysts were kept and sealed on the holder under an argon atmosphere to avoid contact with air and humidity under the characteristic measurement. The spent catalysts were denoted as sCZA-L(CO) and sCZA-

https://doi.org/10.1021/acsomega.2c03068
ACS Omega 2022, 7, 25783−25797

Table 1. Summary of Performance Results for CO and CO_2 Hydrogenation over $Cu/ZnO/Al_2O_3$ (CZA) Catalysts from Our Previous Work[3]

		CO hydrogenation[b]			CO_2 hydrogenation[c]			
catalysts	weight ratio of Cu:Zn[a]	X_{CO}[d] (%)	S_{Mt}[f] (%)	rate of reaction (mol_{CO}/g_{cat} s)	X_{CO_2}[e] (%)	S_{CO}[g] (%)	S_{Mt} (%)	rate of reaction (mol_{CO_2}/g_{cat} s)
CZA-L	0.8	1	100	0.03	1	100	0	0.06
CZA-H	3.0	2	100	0.15	3	99	1	0.18

[a]Results from the ICP-MS analysis. [b]Reaction conditions: T = 250 °C, P = 1 atm, time on stream = 300 min, CO:H_2 = 1:2. [c]Reaction conditions: T = 250 °C, P = 1 atm, time on stream = 300 min, CO_2:H_2 = 1:3. [d]X_{CO} = CO conversion. [e]X_{CO_2} = CO_2 conversion. [f]S_{Mt} = methanol selectivity. [g]S_{CO} = CO selectivity.

H(CO) for CO hydrogenation, while they were designated as sCZA-L(CO_2) and sCZA-H(CO_2) for CO_2 hydrogenation.

2.2.1. X-ray Powder Diffraction (XRD) Analysis. XRD analysis of the spent catalysts after CO and CO_2 hydrogenation reactions (sCZA-L and sCZA-H) was performed with a SIEMENS D-500 X-ray diffractometer using Ni-filtered Cu-Kα radiation as a radiation source. The XRD patterns were recorded in the 2θ range of 20−80° at a scanning rate of 2.4 min^{-1} with a step size of 0.04°. The operating voltage and current were 40 kV and 30 mA, respectively. Phases were identified from XRD patterns using the database from JCPDS (Joint Committee on Powder Diffraction Standards). The average crystalline size (D_{xrd}) was calculated using the Scherrer's equation as follows:

$$D = \frac{K\lambda}{\beta \cos\theta} \quad (1)$$

The Warren's equation was also used

$$\beta = \sqrt{\beta_m^2 - \beta_s^2} \quad (2)$$

The spherical model is assumed for the grains. The crystallites with a cubic shape have K (crystallite-shape factor) ≅ 0.9. λ is the X-ray radiation wavelength (λ = 1.54439 Å). X-ray diffraction broadening (β, radian) is the peak of full width at half maximum (FWHM), which can be obtained by using Warren's equation. According to Warren's equation, β_m is the measured peak width in radians at half peak height, whereas β_s is the corresponding width of a standard material. Finally, θ is the angle of diffraction.

2.2.2. X-ray Photoelectron Spectroscopy (XPS) Analysis. An X-ray photoelectron spectroscopy technique was employed to obtain insights about the chemical states of surface elements. For all elements, there is a characteristic of binding energy associated with the electron configuration of the electrons within the atoms. XPS was carried out using an AMICUS spectrometer with an AlKα spectrometer (1253.6 eV, as an X-ray source) equipped with an AlKα X-ray radiation (1486.6 eV) at a voltage of 15 kV and current of 12 mA. The elemental binding energies (Cu, Zn, Al, and O) were determined with reference to the C 1s line situated at 284.8 eV. The pressure in the analysis chamber was less than 10^{-5} Pa. All measurements were subject to an estimated error of ±0.2 eV.

2.2.3. Temperature-Programmed Reduction (H_2-TPR) Analysis. H_2-TPR was measured in a Micrometric Chemisorb 2750 equipped with a thermal conductivity detector. The catalysts under study (50 mg) were loaded in a quartz reactor (U-shaped) in a continuous flowing system and pretreated in He flow (He flow rate of 25 mL min^{-1}) at 300 °C for 30 min. Then, the sample was cooled down to 30 °C in He to start the reducibility step by 10% of H_2 in Ar. The reduction temperature of H_2 was monitored in the range of 30−500 °C with a heating rate of 10 °C min^{-1} under 10% of H_2 in Ar flow of 25 mL min^{-1}. The amount of H_2 consumption in the effluent was recorded via the thermal conductivity detector (TCD) as a function of temperature.

2.2.4. Specific Surface Area, Pore Volume, and Pore Size Diameter Measurement. The properties of surface parameters of all catalysts were determined by using N_2 adsorption−desorption isotherms. It was measured at the boiling point of liquid nitrogen (−196 °C) over a Micromeritics ASAP-2000 automated system (Micromeritics Instrument Corp., USA). Before the nitrogen physisorption analysis, the catalysts were degassed at 120 °C under nitrogen flow for at least 4 h. The specific surface areas were estimated with the Brunauer−Emmett−Teller (BET) equation, whereas the Barrett−Joyner−Halenda (BJH) method was used to calculate the total pore volume and average pore size diameter.

2.2.5. Energy-Dispersive X-ray Spectroscopy (EDX or EDS). EDX analysis is a surface analytical technique used for the investigation of elemental dispersion and chemical distribution on the surface of catalyst granules. All elemental mappings of the catalyst were also obtained from scanning electron microscopy coupled to energy dispersive spectroscopy (SEM−EDX), in which EDX was performed using an Apollo X Silicon Drift Detector Series by EDAX.

2.2.6. Temperature-Programmed Oxidation (TPO) Analysis. The Micromeritic Chemisorb 2750 automated system and a quartz microreactor (U-shaped) were used for temperature-programmed oxidation (TPO) with a thermal conductivity detector (TCD) to collect the online signal. Approximately 50 mg of spent catalyst was loaded in a quartz reactor and was exposed to 1% oxygen in helium gas (1% O_2/He) using a flow rate of 25 mL min^{-1}. The TPO was performed by raising the temperature from room temperature to 950 °C with a heating rate of 5 °C min^{-1}. The signals of CO and CO_2 were collected by using an online Shimadzu GC-2014 gas chromatograph with Rt-Q-BOND-fused silica PLOT columns every 5 min. However, only CO_2 was detected as the product of the TPO. All TPO data were normalized to the respective sample weight and expressed in arbitrary units.

3. RESULTS AND DISCUSSION

3.1. Catalytic Behaviors and Catalyst Properties after CO and CO_2 Hydrogenation Tests. *3.1.1. Role of Metal Components in the Deactivation Behavior of Catalysts.* Our previous study[3] determined the catalytic activity of $Cu/ZnO/Al_2O_3$ catalysts with different amounts of copper loading, including CZA-L (Cu:Zn = 0.8) and CZA-H (Cu:Zn = 3.0), under atmospheric pressure at 250 °C. These conditions have attracted attention for industrial processes due to their advantage of low energy consumption and low cost, which

https://doi.org/10.1021/acsomega.2c03068
ACS Omega 2022, 7, 25783−25797

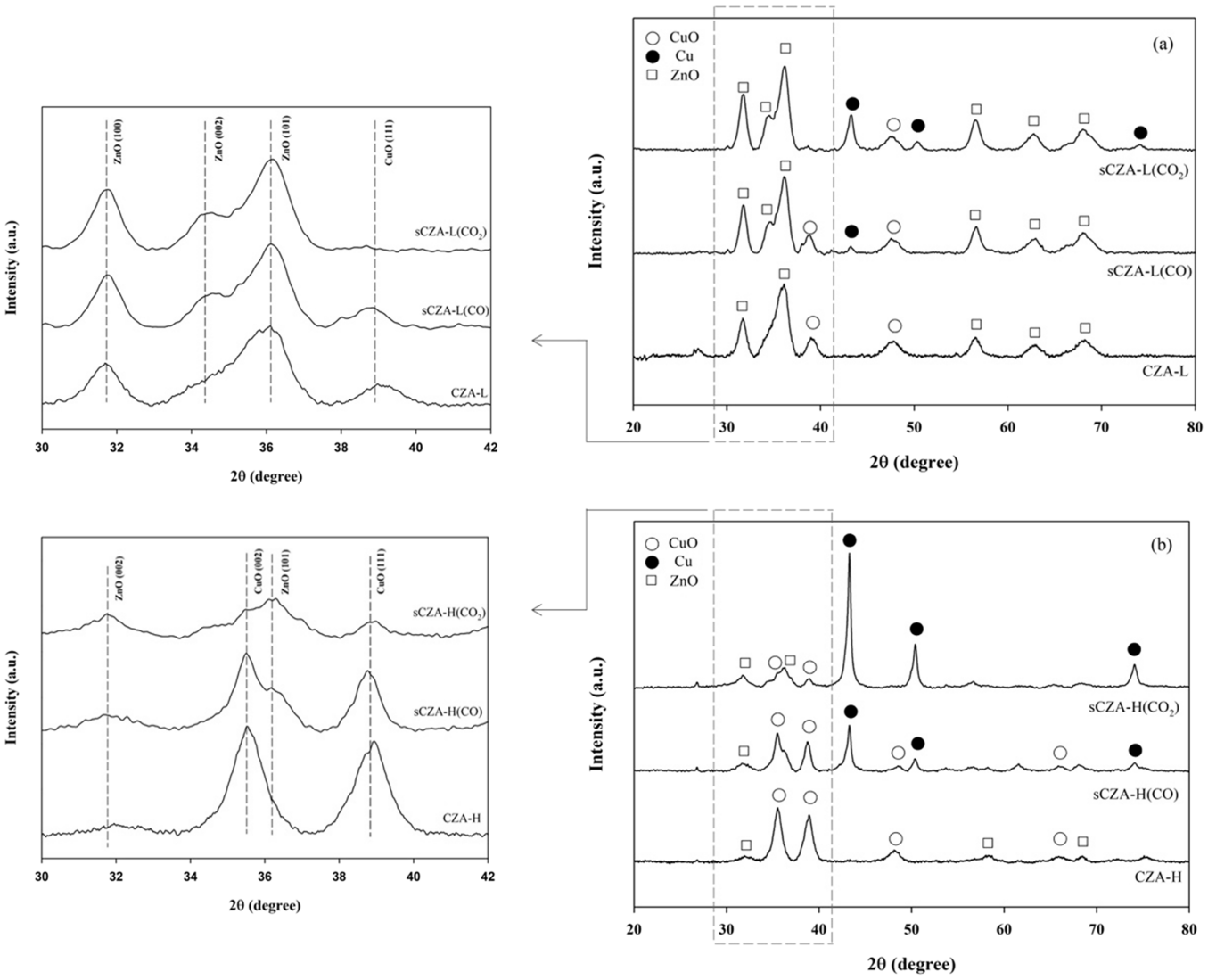

Figure 1. XRD patterns of fresh and spent CZA catalysts: (a) CZA-L (Cu:Zn = 0.8) and sCZA-L and (b) CZA-H (Cu:Zn = 3.0) and sCZA-H.

are facile to control upon CO and CO_2 hydrogenation to methanol.[17,20] It is well known that the high reaction pressure for methanol synthesis from CO or CO_2 hydrogenation results in extremely high energy consumption and high cost of a mechanical process; therefore, more instrument systems must be installed for safety control to prevent the hazards in industrial processes such as process damage, environmental damage, loss of human life, loss of cost, and explosion.[21] Noticeably, the methanol synthesis under low pressure is an alternative route to decrease the cost of manufacturing in terms of the cost of production and technical processes.[3,21] Both catalysts were chosen for catalytic performance screening with time on stream, and the summary of previous results is listed in Table 1. According to previous studies, there are three possible fundamental reactions involved in methanol synthesis via hydrogenation. In the reaction, CO and CO_2 hydrogenation can be divided into three main reactions: CO hydrogenation (eq 3), CO_2 hydrogenation (eq 4), and reverse water-gas shift (RWGS) reaction (eq 5). The reaction equations are described as follows:

$$CO + 2H_2 \leftrightarrow CH_3OH \quad \Delta H_{298K} = -90.84 \text{ kJ mol}^{-1} \tag{3}$$

$$CO_2 + 3H_2 \leftrightarrow CH_3OH + H_2O \quad \Delta H_{298K} = -49.57 \text{ kJ mol}^{-1} \tag{4}$$

$$CO_2 + H_2 \leftrightarrow CO + H_2O \quad \Delta H_{298K} = +41.27 \text{ kJ mol}^{-1} \tag{5}$$

More information of catalyst deterioration in the present work is clarified based on more powerful characterization techniques used to differentiate the changes in characteristics of both fresh and spent catalysts for CZA-L and CZA-H toward CO and CO_2 hydrogenation.

3.1.2. Properties of Metal Sites in Spent Cu/ZnO/Al_2O_3 Catalysts. The XRD patterns of all fresh catalysts (CZA-L and CZA-H) and spent catalysts after the reaction of CO [sCZA-L(CO) and sCZA-H(CO)] and CO_2 hydrogenation [sCZA-L(CO_2) and sCZA-H(CO_2)] are illustrated in Figure 1a,b. In the case of the CZA-L catalyst after reaction testing, sCZA-L(CO) and sCZA-L(CO_2) catalysts showed a high agglomeration of crystallite size. It revealed the increased intensity of ZnO (JCPDS: 36-1451 with diffraction peaks at 2θ = 31.8, 36.4, 56.6, 62.9, and 68.0°) and generated the ZnO peak at ≈34.4° by comparison with fresh CZA-L.[22,23] On the other hand, the peaks of CuO (JCPDS: 48-1548, diffraction peaks at

https://doi.org/10.1021/acsomega.2c03068
ACS Omega 2022, 7, 25783−25797

Table 2. Physicochemical Properties of Cu/ZnO/Al_2O_3 (CZA) Catalysts

	crystallite size[b] (nm)				N_2 physisorption	
catalyst	D_{CuO}	D_{Cu}	D_{ZnO}	BET surface area[c] (m^2/g)	pore volume[d] (cm^3/g)	pore size (nm)
fresh catalyst[a]						
CZA-L	4.9		7.2	49.5	0.3	16.9
CZA-H	8.7		3.9	77.5	0.5	17.4
spent catalyst						
sCZA-L(CO)	4.5	7.5	10.0	38.3	0.1	12.7
sCZA-H(CO)	5.5	15.3	5.4	50.0	0.2	15.6
sCZA-L(CO_2)	3.4	9.3	9.5	26.9	0.1	15.7
sCZA-H(CO_2)	3.6	22.3	4.7	61.5	0.3	14.9

[a]Previous work.[3] [b]Determined by the intense XRD reflection peak according to the Scherrer's equation based on the reflection of the (111) and ($\bar{2}$02) planes at 2θ = 38.7 and 48.8° for CuO, (111) and (200) planes at 2θ = 43.4 and 50.5° for Cu, and (100) and (101) planes at 2θ = 31.9 and 36.3° for ZnO. [c]Specific surface area of the catalysts via the N_2 physisorption method. [d]Determined by the BJH desorption method.

2θ = 35.6, 38.7, 48.8, 61.6, and 66.2°) for spent (sCZA-L) catalysts after both hydrogenation reactions became broader and weaker.[24,25] Moreover, the Cu metal phase (Cu^0) as the diffraction peaks at 2θ = 43.4, 50.5, and 74.1° (JCPDS: 04-0836) is also observed in all sCZA-L catalysts, especially in sCZA-L(CO_2).[22,24] In contrast, ZnO species was decreased (31.8°) and did not appear for some ZnO diffraction peaks (61.6 and 66.2°) on the spent CZA-H after CO and CO_2 hydrogenation [sCZA-H(CO) and sCZA-H(CO_2)] compared to the fresh CZA-H catalyst. Considering CuO and Cu species in all sCZA-H catalysts, the peak of CuO in fresh CZA-H tended to decrease after the CO and CO_2 hydrogenation testing in time on stream, while the peaks corresponding to metallic copper (2θ = 43.4, 50.5, and 74.1°) noticeably occurred. From the results above, the metal species agglomeration occurred over sCZA-L(CO) and sCZA-L(CO_2) by blockage of CuO and ZnO surface sites, which resulted in the low catalytic activity[3] and is also the cause of the catalyst deactivation. In comparison involving the effect of copper loading, the Cu^0 species of sCZA-L(CO) and sCZA-L(CO_2) catalysts were present as a small peak, while the strong sharp peak of Cu^0 was obtained from sCZA-H(CO) and sCZA-H(CO_2). It indicated a success in reducing Cu^{2+} into Cu^0 species, which act as the main active site for methanol production in the hydrogenation reaction of CO and CO_2.[3,26,27] Additionally, the average crystallite sizes of ZnO (at 2θ = 31.9 and 36.3°), CuO (at 2θ = 38.7 and 48.8°), and Cu^0 (at 2θ = 43.4 and 50.5°) calculated from the Scherrer's equation were determined for all catalysts and are summarized in Table 2. As calculated by the Scherrer's equation (eq 1), the CuO crystallite sizes of all spent CZA catalysts [sCZA-L(CO), sCZA-L(CO_2), sCZA-H(CO), and sCZA-H(CO_2)] were smaller than those of fresh CZA catalysts (CZA-L and CZA-H) due to the large ZnO crystallites that may cover some surface of CuO, especially sCZA-L(CO_2). It can be confirmed that the ZnO crystallite sizes became larger in the spent CZA catalysts. Furthermore, the decreased CuO sizes of fresh CZA catalysts were then reduced to form Cu^0 after the H_2 reduction process ($CuO + H_2 \rightarrow Cu^0 + H_2O$) and during the hydrogenation testing. However, the ZnO crystallite size of spent CZA-L catalysts in both CO and CO_2 hydrogenation is increased by more than 32% when compared with fresh CZA-L. This is because ZnO was agglomerated during the reaction and resulted in a decrease in the catalytic activity by ZnO blocking the Cu surface from contact with the feed gas. In addition, the Cu^0 crystallite size for spent CZA catalysts is in the order sCZA-H(CO_2) > sCZA-H(CO) > sCZA-L(CO_2) > sCZA-L(CO). As a result, the small Cu crystallite size of sCZA-L(CO) and sCZA-L(CO_2) is attributed to the effect of ZnO. It should be noted that these factors have an effect on the structural changes during the CO and CO_2 hydrogenation reaction for 300 min. Comparing spent CZA catalysts for CO and CO_2 hydrogenation, the characteristic peaks of CuO for sCZA-L(CO_2) and sCZA-H(CO_2) were less intense than the diffraction peaks for sCZA-L(CO) and sCZA-H(CO), while the Cu^0 peaks were more pronounced. This was attributed to the Cu formation that was clearly noticeable and completely reduced from CuO to Cu^0, corresponding to the larger Cu crystallite size in spent catalysts after the CO_2 hydrogenation. Furthermore, the lower intensity of Cu^0 peaks in spent catalysts for CO hydrogenation [sCZA-L(CO) and sCZA-H(CO)] was possible for the indication of partial reoxidation behavior (Cu^0 to CuO) during CO hydrogenation testing. From the results of ZnO crystallite size, the ZnO crystallite sizes of sCZA-L(CO) and sCZA-H(CO) were slightly larger those of sCZA-L(CO_2) and sCZA-H(CO_2), suggesting a decrease in the crystallite size of Cu, as shown in Table 2. A change in surface morphology occurred, which likely influenced the stabilization of Cu^0 species in partially different oxidation states according to several authors.[28,29] It is well known that the CO in the feed of hydrogenation results in the formation of inactive Cu sites; hence, the unstable Cu^0 site and smaller crystallite size of Cu^0 can be obtained from sCZA-L(CO) and sCZA-H(CO).[28]

XPS measurements were performed to examine the changes in the chemical state of metal species on the surface with different Cu loadings for synthesized CZA catalysts after testing in the CO and CO_2 hydrogenation (spent catalysts). XPS spectra were collected from the few top layers of the catalyst, and the atomic concentrations were determined. The spectra were acquired in the electron binding energy (BE) regions and are presented in Figure 2a,h. Many researchers suggest the effect of accumulation of O species. It can dissociate to CO, CO_2, and H_2 intermediates on ZnO or Cu^0 metal sites.[9,30] This fact promoted the mechanism of HCOO and O intermediates of changing methanol. For the chemical state of Cu^{2+} (Cu−O species) in Figure 2a,b, the peaks located at 935.6 ± 0.7 eV and 954.9 ± 0.7 eV belong to Cu $2p_{3/2}$[31] and Cu $2p_{1/2}$,[32] respectively. Moreover, two characteristic binding energy (BE) peaks located in the range values of 942−944 eV and 962−964 eV correspond to the shake-up Cu 2p satellite peaks, which confirmed the presence of Cu^{2+} species.[33,34] This is because of the charge transfer between the 3d orbital of the transition metal and the 2p orbital of surrounding ligand

https://doi.org/10.1021/acsomega.2c03068
ACS Omega 2022, 7, 25783−25797

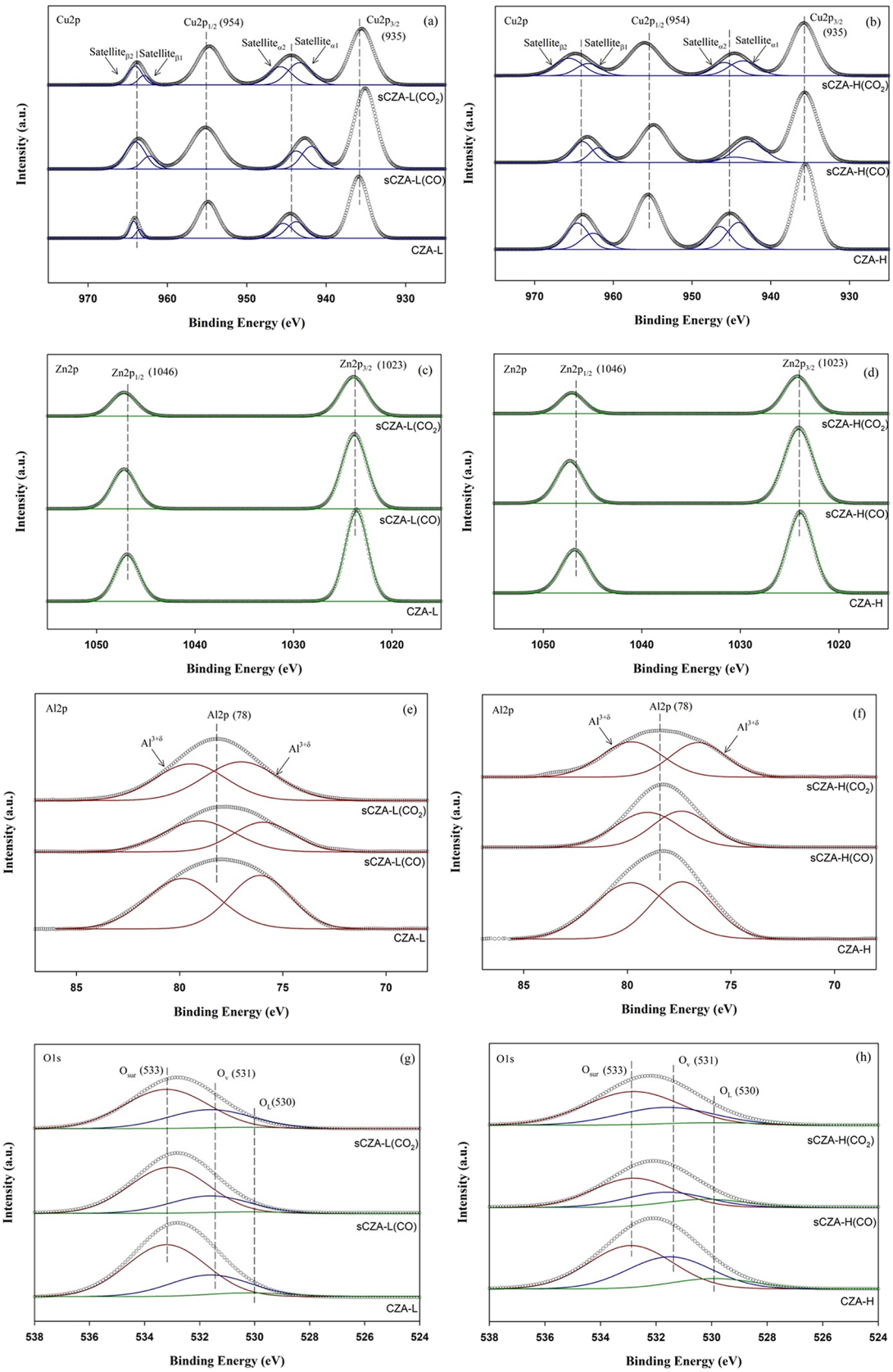

Figure 2. XPS spectra for fresh and spent CZA-L (Cu:Zn = 0.8) catalysts: (a) Cu 2p, (c) Zn 2p, (e) Al 2p, and (g) O 1s. XPS spectra for fresh and spent CZA-H (Cu:Zn = 3.0) catalysts: (b) Cu 2p, (d) Zn 2p, (f) Al 2p, and (h) O 1s.

oxygen.[33] The Zn $2p_{3/2}$ and Zn $2p_{1/2}$ XPS peaks (as seen in Figure 2c,d) have binding energies ≈1023 eV and ≈1046 eV, respectively. These peaks of Zn species are attributed to Zn^{2+} species in bulk ZnO on the catalyst surface.[35,36] Furthermore,

https://doi.org/10.1021/acsomega.2c03068
ACS Omega 2022, 7, 25783−25797

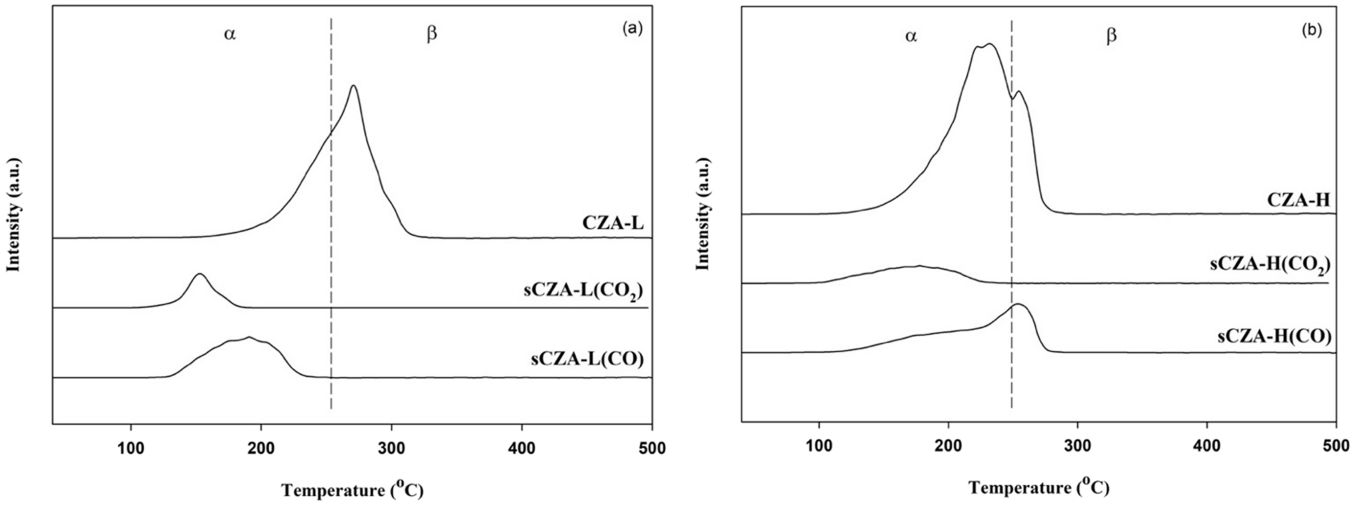

Figure 3. H_2-TPR profiles of fresh and spent CZA catalysts: (a) CZA-L (Cu:Zn = 0.8) and sCZA-L and (b) CZA-H (Cu:Zn = 3.0) and sCZA-H.

Table 3. H_2 Reduction Peak Position and the H_2 Consumption of Fresh and Spent Catalysts in the Temperature-Programmed Reduction (TPR)

catalysts	$T_{\alpha1,\alpha2}$ (°C)	T_{β} (°C)	H_2 consumption (mmol/g_{cat})	% H_2 consumption of spent/fresh	% dispersion of Cu
fresh catalysts					
CZA-L		271	3.8		18.2
CZA-H	205, 233	259	8.7		22.6
spent catalysts					
sCZA-L(CO)	194		1.5	39.4	6.2
sCZA-H(CO)	189	259	2.9	33.3	8.0
sCZA-L(CO_2)	157		0.7	18.4	3.3
sCZA-H(CO_2)	178		1.4	16.1	3.8

the peak appeared at ≈78 eV in Figure 2e,f for all catalysts, corresponding to the characteristic peak of Al 2p spectra ($Al^{3+\delta}$ species).[17,37,38] This is shifted from low to high binding energy when compared to the original peak for pure Al_2O_3 (Al^{3+} species, 74.1 eV), according to previous literature studies.[37,38] As reported by Li et al.[38] and Fu et al.,[37] they explained that the shifted higher binding energy occurred from the chemical state of some Al^{3+} species that increased to the state of $Al^{3+\delta}$ species to maintain the loss of electron because of Cu interacting with Al_2O_3 (Al−O−Cu bond). However, these results showed similarity since the amount of Al_2O_3 that is altered in the catalyst is very low. From Figure 2g,h, the XPS of O 1s spectra are also analyzed to determine the surface oxygen property change where all catalysts showed three peaks after deconvolution in range of 528−535 eV. The chemical state of O 1s can be subdivided into three peaks, which are located at 530 ± 0.2, 531 ± 0.4, and 533 ± 0.4 eV for both fresh (CZA-L and CZA-H) and spent catalysts [sCZA-L(CO), sCZA-L(CO_2), sCZA-H(CO) and sCZA-H(CO_2)] after CO and CO_2 hydrogenation. The first peak around 530 ± 0.2 eV is ascribed to the XPS peak of lattice oxygen of metal oxides (O_L).[39,40] The second peak at 531 ± 0.4 belongs to oxygen vacancy (O_v) in the metal oxide, and the peak at 533 ± 0.4 is attributed to the surface chemisorbed oxygen (O_{sur}).[40,41] The low intensity broad peak of the lattice oxygen of metal oxides (O_L) indicated that the corresponding CZA catalyst has a weak interaction between Cu species and Al_2O_3.[41] The binding energy of O 1s for all catalysts is nearly similar; therefore, it does not have directly significant effects on the surface properties. In the case of spent CZA catalysts, the Cu^{2+} species were strongly decreased, especially sCZA-H(CO) and sCZA-H(CO_2) that have decreased peak intensity of Cu 2p and the shake-up satellite species. It can be confirmed that the decrease in shake-up satellite species resulted in the loss of Cu^{2+} species from the surface catalysts.[33] On the other hand, the XPS spectra of Cu 2p for the lower Cu loading in spent catalysts [sCZA-L(CO) and sCZA-L(CO_2)] exhibited increased peak intensity and a higher peak of satellite and satellite phase. This is due to the agglomeration of Cu species on the surface that occurred via the partial reoxidation to form CuO species during the hydrogenation reaction, especially on the sCZA-L(CO) catalyst.[33] Additionally, the BE of Cu $2p_{3/2}$ species slightly shifted to lower BE values, which suggest the increase in the electron density of Cu species, whereas the XPS spectra of Zn $2p_{3/2}$ and Zn $2p_{1/2}$ slightly shifted to higher BE values. It can be clarified by the subsistence of charge transfer from ZnO to metal Cu for all spent catalysts.[35,42] This result was denoted in the metal interface interaction (Cu-ZnO interaction). It promoted the ZnO interaction of the CZA catalyst, and a change in deconvoluted peak was not observed in Cu^{2+}. However, the opposite shifts of BE values between Cu 2p and Zn 2p spectra indicate the strong interaction of Cu-ZnO over sCZA-L(CO) and sCZA-L(CO_2), leading to a harder reduction of Cu^{2+} to Cu metal (this catalyst behavior is related to the results of H_2-TPR, and details are provided in the next section). This reason suggests the stability of Cu^{2+} active sites to Cu^0. In our observation, the XPS result can describe the surface behavior that affects the catalyst deactivation by metal agglomeration and metal-support arrangement. It is the reason that led to the inactive forms

https://doi.org/10.1021/acsomega.2c03068
ACS Omega 2022, 7, 25783−25797

of CuO and ZnO on the catalyst surface with large active sites for sCZA-L after being used in both CO and CO_2 hydrogenation reactions.

The consumed amount of H_2 was examined to describe the reduction behavior of catalysts by H_2 temperature-programmed reduction (H_2-TPR). Generally, H_2-TPR is a highly sensitive technique to detect and analyze the reduction stage of metal species and amounts of substances. The H_2-TPR profiles of the fresh and spent catalysts with different Cu contents are depicted in Figure 3a,b, whereas Table 3 presents the amount of H_2 consumption. Obviously, all Cu-based catalysts presented a H_2 asymmetric reduction peak in the range of 100−300 °C, which exhibited two predominant H_2 reduction peaks. Two reduction peaks in the TPR profiles are assigned to the chemical environment of CuO species with several states:[3] (i) the reduction peak at the lower temperatures below 250 °C (α peak) is attributed to the highly dispersed CuO, suggesting the strong interaction between Cu and ZnO[22,43] and (ii) the high temperature reduction peak (β peak) is ascribed to the reduction of bulk CuO (core layer of CuO, CuO → Cu_2O → Cu^0) and the interaction of isolated CuO in bulk ZnO.[1,3,22,23] As presented in Figure 3a,b, the reduction peaks of all spent catalysts exhibited similar kinds of reduction patterns with a single peak, except for CZA-H(CO) that showed two peak regions the same as the fresh CZA-H catalyst. It is possibly generated from the presence of several different copper oxide species. Moreover, the H_2-TPR profiles (α peak and β peak) of all spent catalysts were shifted from high to low temperatures and became weaker after the CO and CO_2 hydrogenation testing for 300 min in comparison to fresh CZA catalysts. It was reported that the reduction behavior of CuO particles in different peak positions is related to the CuO grain size and the interaction of CuO with other metal oxides.[44,45] These results of spent catalysts inferred that the crystallite size of CuO decreased, which are in good agreement with those obtained from XRD measurements as listed in Table 2 in comparison to fresh catalysts.[33,35] However, the reduction peaks also depend upon the different strength interactions between CuO and ZnO, resulting in the reduction peaks of sCZA-L in CO and CO_2 hydrogenation appearing in a higher temperature despite small CuO crystallite sizes, as shown in the XRD results. It is noteworthy that the change of the interaction between CuO and ZnO particles was related to the activity of Cu sites generated during the hydrogenation reduction. After the CO and CO_2 hydrogenation testing, the CuO species in CZA catalysts were not completely reduced into metallic copper and some Cu^0 can be transformed back to CuO by the reoxidation pathway during the reaction testing.[33,46] In other words, the copper species of both CuO and Cu^0 existed in spent catalysts as confirmed by the characteristic peaks in XRD results. In addition, it can be also ascribed to the shift of the H_2-TPR peak caused by the change in electron density of copper during the hydrogenation reaction as proven by following the shifting in binding energy of Cu−O in XPS results (Figure 2a,b).[34] In addition, the reduction peak intensity of all spent catalysts from CO and CO_2 hydrogenation was dramatically decreased, especially for the sCZA after CO_2 hydrogenation. This is because of the Cu^0 that is very stable during the reaction or a loss of CuO site. In order to know more clearly about the hydrogen adsorption capacity of the catalysts, the H_2 consumption of each catalyst is shown in Table 3. The percentage of H_2 consumption for the four spent catalysts was observed in the following order: sCZA-L(CO) > sCZA-H(CO) > sCZA-L(CO_2) > sCZA-H(CO_2), suggesting that the Cu^0 sites of CZA catalysts having lower Cu contents may undergo reoxidation during the CO and CO_2 hydrogenation. Furthermore, these results indicated that the hydrogen consumption of spent CZA catalysts in both hydrogenation reactions decreased with the increase in the number of Zn contents in catalyst composition [sCZA-L(CO) and sCZA-L(CO_2)], contributing to the dwindling of CO and CO_2 hydrogenation ability. According to the literature studies,[1,4,17,47,48] the stability of Cu^0 sites during the CO and CO_2 hydrogenation is the main key factor for H_2 dissociation to adsorb feed molecules in the product formation step, resulting in the increase in the catalytic ability of Cu-based catalysts. In addition, the high Zn contents in the catalyst result in the formation of more surface Zn sites and blocking of the formation of Cu-ZnO interfaces, which acted as a source of the H atom storage for the intermediate molecules in the hydrogenation process. This finding demonstrated that the Cu-based catalyst having high stability of Cu^0 sites results in the high catalytic stability for only focusing the metal active sites. Therefore, the results of the higher catalytic activity and stability of active metal were obtained from CZA catalysts having a higher Cu loading (Cu:Zn = 3.0, CZA-H).

Considering the effects of physicochemical properties on catalytic performance, the dispersion of copper over all the catalysts is illustrated in Table 3. The results showed that the calculated Cu dispersion is 22.9% for CZA-H, whereas the increasing ZnO loading in the CZA-L catalyst resulted in a lower dispersion of Cu particles (ca. 18.2%). However, after the hydrogenation reaction, some Cu crystallites tended to agglomerate, corresponding to the decrease in Cu dispersion from 23−18% to 3−8% compared to the CZA catalyst prior to reaction testing. In order to further evaluate the catalytic stability, the percentage of Cu dispersion for spent CZA catalysts after testing in both reactions is in the order sCZA-H(CO) (ca. 8.0%) > sCZA-L(CO) (ca. 6.2%) > sCZA-H(CO_2) (ca. 3.8%) > sCZA-L(CO_2) (ca. 3.3%), suggesting that the Cu dispersion of spent catalysts was not obviously different and the effect of Cu loading is insignificant upon the agglomeration of CuO in spent catalysts. Nevertheless, the Cu dispersion of the catalyst having high Cu contents (sCZA-H) is still slightly high when compared to sCZA-L. According to the crystallite size of Cu from the XRD results of spent CZA catalysts, D_{Cu} values of sCZA-L(CO_2) and sCZA-H(CO_2) are higher than those of sCZA-L(CO) and sCZA-H(CO). It indicated that some Cu particles and ZnO particles were possibly aggregated to form particles with large sizes, leading to a decrease in Cu dispersion.[46] In addition, the relationships between catalytic activity and Cu dispersion in both CO hydrogenation and CO_2 hydrogenation reactions are shown in Tables 1 and 3, respectively. The amount of Cu loading had a significant effect on the catalytic activity (CO and CO_2 conversion). As shown in Table 3, the high Cu dispersion can promote the catalytic activity in terms of reaction rate (Table 1) with the higher Cu loadings in the CZA catalyst. The high Cu dispersion (18.2%) obtained from the CZA-H catalyst resulted in the enhancement of reaction rates for both CO and CO_2 hydrogenation that were around 0.15 mol of $CO \cdot g_{cat}^{-1} \cdot s^{-1}$ and 0.18 mol of $CO_2 \cdot g_{cat}^{-1} \cdot s^{-1}$, respectively. This is because Cu is the active metal, whereas ZnO acts as a metal promoter that facilitates the stability and dispersion of copper. From this observation, the amount of ZnO added into CZA catalysts should be appropriate to avoid the agglomeration of

https://doi.org/10.1021/acsomega.2c03068
ACS Omega 2022, 7, 25783−25797

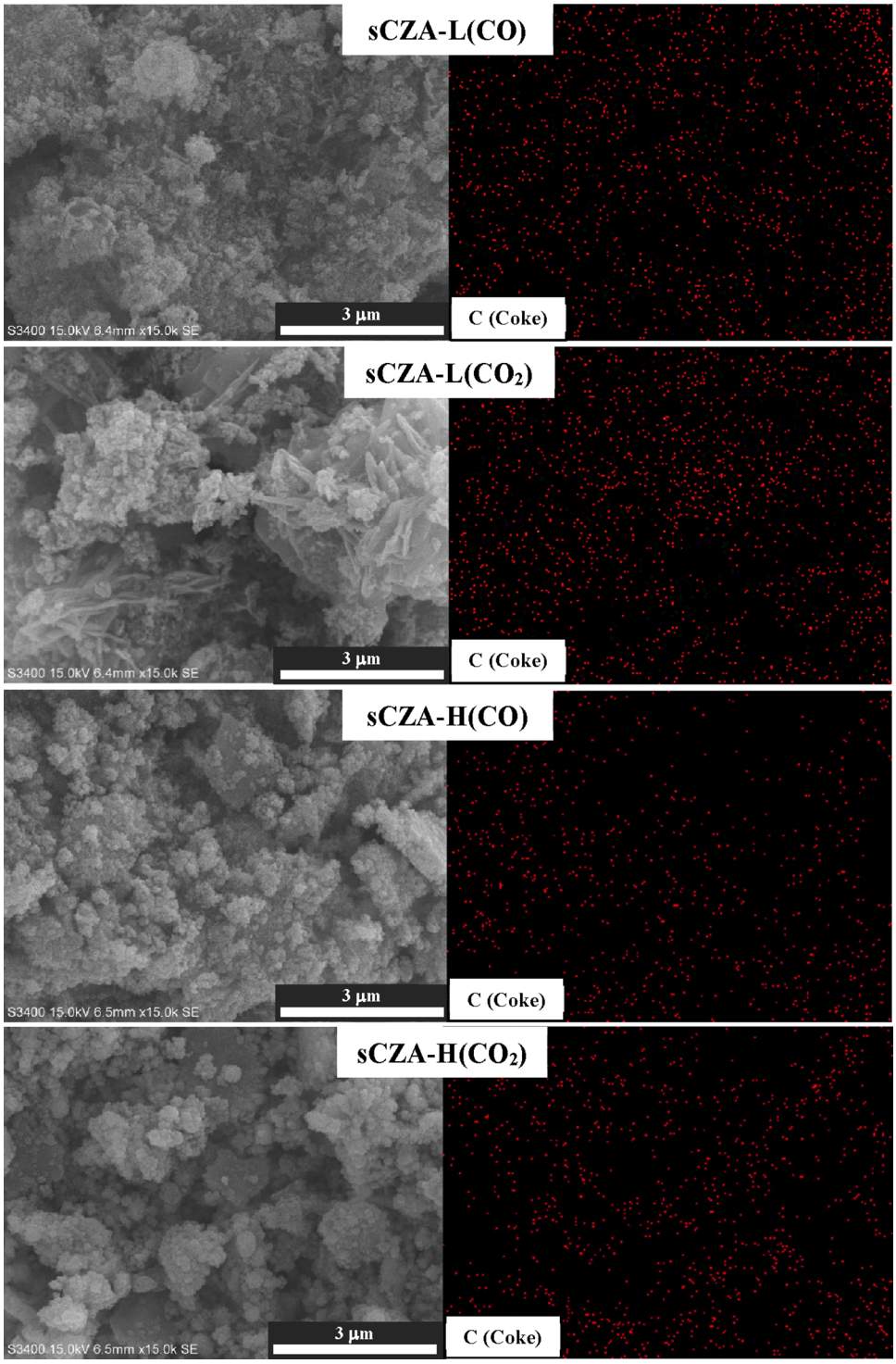

Figure 4. EDX mapping of spent CZA catalysts: sCZA-L(CO), sCZA-L(CO_2), sCZA-H(CO), and sCZA-H(CO_2).

ZnO, which leads to a decrease in catalytic activity and an increase in the catalytic deterioration.[1,26] However, there was no significant difference in the observed catalytic activity when comparing between CO and CO_2 in the feed of hydrogenation.

In view of the above discussion for this section, the results from the behavior of metal active sites (XRD, XPS, and H_2-TPR characterization) could be explained by the aggregation of the metal nanoparticles (Cu and ZnO particles) and the unstable Cu^0 active sites from the reoxidation to Cu^+ and Cu^{2+} during the CO and CO_2 hydrogenation reaction, which confirmed the cause of catalytic deactivation for the CZA catalyst.[1,46] Additionally, the change of metal surface behavior corresponds to the change of the surface areas obtained from the N_2 physisorption, which will be elucidated in the next section. This characteristic was significantly vital to determine the deeper reason of catalyst deactivation for high Zn contents in CZA catalysts [sCZA-L(CO) and sCZA-L(CO_2)].

3.2. Structural Characterization and Identification of the Coke Formation in the Spent Catalyst. In this section, a comprehensive discussion regarding deactivation processes

https://doi.org/10.1021/acsomega.2c03068
ACS Omega 2022, 7, 25783−25797

Table 4. Element Distribution from EDX Analysis in Fresh and Spent $Cu/ZnO/Al_2O_3$ (CZA) Catalysts

	weight percentage of element (wt %)					
	fresh		CO hydrogenation		CO_2 hydrogenation	
element	CZA-L	CZA-H	sCZA-L(CO)	sCZA-H(CO)	sCZA-L(CO_2)	sCZA-H(CO_2)
Cu	42.3	70.0	41.2	68.3	40.4	68.8
Zn	53.0	24.5	51.9	24.9	50.1	24.7
Al	4.7	5.5	4.0	5.4	5.2	4.7
C			2.9	1.4	4.3	1.8
loss of Cu (%)			2.6	2.4	4.5	1.7

by carbon and coke deposition over CZA catalysts upon different Cu loadings via CO and CO_2 hydrogenation with physical deposition was given. It is well-known that carbon and coke formation are mostly referred as a result of the corresponding CO and CO_2 dissociation and/or decomposition of hydrocarbons reaction over solid catalysts, which resulted in the blockage of active sites and surface on solid catalysts, consequently causing a decrease in catalytic ability.[14] The coke deposition can be probably formed by two main deactivation mechanisms, namely, the Boudouard reaction (eq 6) and the reduction of CO (eq 7).[16,49] The Boudouard reaction (eq 6) is the disproportion of CO (as a carbon source) into CO_2 and coke (i.e., amorphous coke and graphitic coke), while eq 5 is the reduction of CO with H_2 to form the carbon (C) atom and water (reverse carbon gasification). Both of these mechanisms of coking are more favorable at lower temperatures and the two reaction mechanisms take place as follows:

$$2CO \leftrightarrow C + CO_2 \quad \Delta H_{298K} = -173.30 \text{ kJ mol}^{-1} \tag{6}$$

$$CO + H_2 \leftrightarrow C + H_2O \quad \Delta H_{298K} = -131.30 \text{ kJ mol}^{-1} \tag{7}$$

Dispersive X-ray spectroscopy (EDX) was also performed to examine the elemental distribution on the surface of the fresh and spent CZA catalyst, according to our previous work.[3] The elemental mappings in the catalyst samples reveal the metal distribution as shown in Figure 4. It can be detected by using the EDX mapping mode, in which the distributions of Cu, Zn, Al, and C (coke) atoms were observed. The elemental mappings for distribution of Cu, Zn, and Al of all fresh catalysts (CZA-L and CZA-H) and all spent catalysts [sCZA-L(CO), sCZA-L(CO_2), sCZA-H(CO), and sCZA-H(CO_2)] in a particular region are presented in the Supporting Information Figures S2−S7. The density of Cu was strongly observed in fresh and spent CZA-H because Cu is the main component (Figures S5−S7). On the contrary, the EDX mapping of both fresh and spent CZA-L catalysts mainly presented the Zn distribution (Figures S2−S4). After reaction testing in CO and CO_2 hydrogenation, the distribution of the carbon atom was generated. In order to investigate the effect of different Cu loadings, the carbon atom on the surface of all spent catalysts showed similar distribution, but the amount of carbon deposition of spent catalysts having lower Cu loadings [sCZA-L(CO) and sCZA-L(CO_2)] was more than twice. This can be explained by not only the agglomeration of metal and metal oxide particles but also the coke formation (carbon atom) that can cover the active site, showing the loss of active surface, resulting in the deactivation CZA catalysts during the CO and CO_2 hydrogenation. In fact, several authors have proven that carbon deposition on catalysts providing the active site is inactive and decreases the catalytic activity,[28,50] according to the catalytic activity results in our previous work.[3] In addition, the carbon deposition results as shown in Table 4 (from our previous report,[3]) provide the content of metal elements including Cu, Zn, Al, and C in fresh and spent CZA catalysts. These results confirmed the decrease in some Cu metal concentration on the surface of the sCZA catalyst from the blockage of carbon deposition, especially in sCZA-L(CO) and sCZA-L(CO_2) as presented by the decrease in the BET surface area from N_2 physisorption analysis, which was attributed to the leaching of Cu during the reaction.

The BET surface area, pore volume, and average pore size diameter of fresh and spent catalysts in CO and CO_2 hydrogenation are presented in Table 2. Considering the BET specific surface area, all spent catalysts after being used in both CO and CO_2 hydrogenation showed lower BET surface areas when compared to fresh catalysts. The considerable BET surface area of catalysts having low Cu loadings after CO_2 hydrogenation [sCZA-L(CO_2)] had a dramatic decrease up to 46% (49.5 to 26.9 m^2/g as seen in Table 2), while the decrease in the specific surface area of other spent catalysts was in the range of 20 to 35%. Considering the pore volume and average pore diameter of the spent catalysts, they showed slightly lower values, except for the pore volume of sCZA-L(CO) that decreased up to 25%. These structural characterization results of the spent catalysts showed that the decreased surface area and pore volume occurred from the loss of surface active sites during methanol synthesis (CO and CO_2 hydrogenation), especially in sCZA-L(CO_2). Furthermore, these results also suggest that the decrease in the catalyst surface and structure was caused by the deactivation of the catalyst, resulting in the lower catalytic activity of CZA catalysts with low Cu loadings [sCZA-L(CO) and sCZA-L(CO_2), as shown in Table 1].[19] This can be reasonably attributed to the lower loading ratio of the Cu:Zn (ca. 0.8) in sCZA-L(CO) and sCZA-L(CO_2), in which the blockage of the surface structure by the carbon atom was confirmed by EDX results. However, the confirmation of catalytic deactivation by the presence of carbonaceous species was also analyzed by a temperature-programmed oxidation (TPO) for better understanding.

The nature and the amount of coke formation on the catalyst surface after CO and CO_2 hydrogenation were determined by the temperature-programmed oxidation (TPO) analysis, as seen in Figure 5. The coke combustion profiles on the spent catalysts (TPO profiles) cover a range of temperatures from 50 to 950 °C, suggesting the different types of coke deposition that were deconvoluted by the Gaussian peak fitting method. It showed two temperature ranges of different carbonaceous species as follows: (i) the peak at lower temperatures below 500 °C (coke I) is assigned to soft coke (a uniform and amorphous coke), which can be removed by a suitable decoking process to regenerate surface sites and (ii) the second one at high temperatures above 500 °C (coke II) is

https://doi.org/10.1021/acsomega.2c03068
ACS Omega 2022, 7, 25783−25797

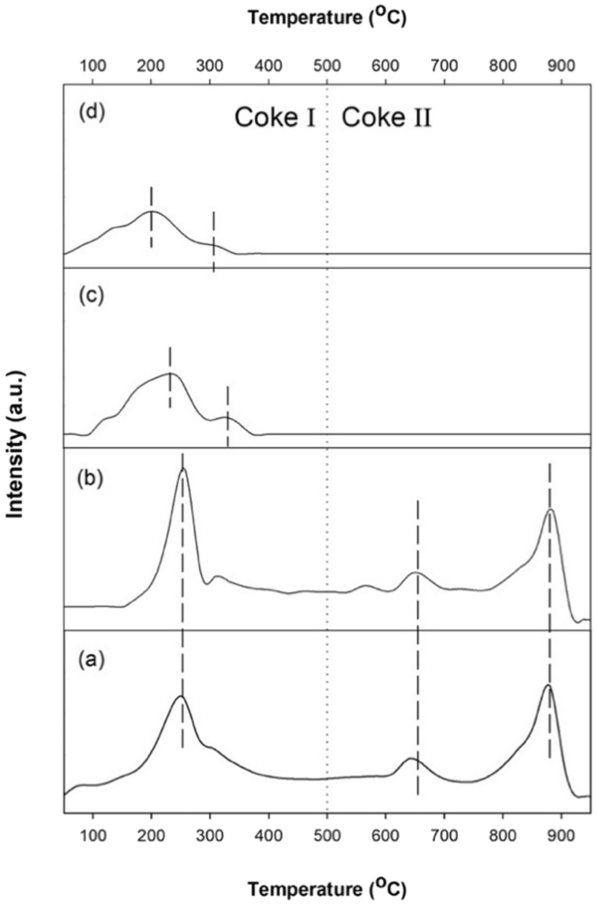

Figure 5. Effect of different Cu loadings in the CZA catalysts on the TPO profiles for fresh and spent CZA catalysts: (a) sCZA-L(CO), (b) sCZA-L(CO_2), (c) sCZA-H(CO), and (d) sCZA-H(CO_2).

attributed to hard coke (carbon filaments or graphitic coke), resulting in the decrease in the reaction rate by losing the intrinsic catalyst surface site because this coke species is difficultly eliminated from catalyst particles;[19,51] therefore, this resulted in the permanent catalytic deactivation and more rapid deactivation. The TPO profiles of sCZA-H(CO) and sCZA-H(CO_2) are similar, which exhibited two overlapping peaks centered below 500 °C in ranges of 200−250 and 310−325 °C, corresponding to an amorphous coke that covers the surface sites.[51] On the other hand, sCZA-L(CO) and sCZA-L(CO_2) presented one peak at lower temperatures (≈256 °C) and two peaks at high temperatures (>500 °C). As known, the coke contents that burn below 500 °C can be related to a low deactivating coke (a uniform and amorphous coke) that is retained on Cu metallic sites of the catalyst.[19,50,51] This coke species is easier to remove or modify during the hydrogenation reaction or it can be removed during regeneration. Accordingly, many researchers explained the fundamental catalytic regeneration on the surface in terms of surface reversibility in H_2, steam, or CO_2 and activated oxygen over the surface sites by Argyle and Bartholomew[14] and Wu et al.[52] Therefore, the active sites (Cu metallic) can be reactivated to catalyze product formation that results in the high catalytic activity of the CZA catalyst with high Cu contents (CZA-H). It would be extremely useful to make them highly stable, resulting in the prolonged lifetime of catalysts. For the combustion at temperatures above 500 °C in sCZA-L(CO) and sCZA-L(CO_2), with well-defined and centered peaks at ≈660 and ≈880 °C, it is assigned to the highly deactivating coke (hard coke or graphitic nature of coke) deposited on metallic sites that decreased the surface area of CZA catalysts by the blockage of the metallic sites, especially in sCZA-L(CO) and sCZA-L(CO_2).[14] Additionally, the quantification of coke contents on all spent catalysts is summarized in Table 5 and

Table 5. Amount of Coke Deposition over Spent Cu/ZnO/Al_2O_3 (CZA) Catalysts in the Temperature-Programmed Oxidation (TPO)

catalysts	total coke deposition (%)
CO hydrogenation	
sCZA-L(CO)	2.19
sCZA-H(CO)	0.30
CO_2 hydrogenation	
sCZA-L(CO_2)	2.63
sCZA-H(CO_2)	0.44

calculated by integrating the area under coke combustion peaks. The percentages of coke content in sCZA-H(CO) and sCZA-H(CO_2) are 0.30 and 0.44%, respectively. In the case of the catalysts having high Zn contents, the coke contents in sCZA-L(CO) and sCZA-L(CO_2) are 2.19 and 2.63%, respectively. As mentioned above when explaining the result in Table 5, this could be related to the lower conversion of CO and CO_2 in the hydrogenation reaction for higher Zn contents in the CZA catalyst (CZA-L), which are presumably more favorable in the formation of hard coke (graphitic coke). Furthermore, the higher content of soft coke and hard coke would suppress the reactions of product formation as the blockage of active sites and the opportunity of feed gas contact with Cu metallic sites will be hindered by the coke formation. To clarify the coke deposition behavior with the effect of Cu content in catalysts, the coke formation determined by TPO analysis of the spent catalysts was in agreement with that obtained from the thermogravimetric (TGA) technique reported in our previous work.[3] As well known, TGA is commonly performed to quantify the coke deposition on the spent catalysts after CO and CO_2 hydrogenation as well as other techniques. The TGA results were reported in our previous work,[3] in which it described the coke formation and types in terms of weight loss upon increased temperature. Both techniques showed similar results having two groups of carbon species, including amorphous carbon and graphitic carbon. Moreover, the high amount of coke was observed from sCZA-L after both CO and CO_2 hydrogenation reactions having values of 2.3 and 3.1% using the TGA technique, respectively. However, the low amounts of coke were ca. 0.8 and 0.9% in sCZA-H(CO) and sCZA-H(CO_2), respectively. It revealed that the CZA-H catalyst exhibited high catalytic activity in both CO and CO_2 hydrogenation reactions due to the high Cu content and high Cu dispersion (as seen in Table 3), which retarded the carbon formation (anti-coking ability).[17,28] In addition, the deactivation of CZA catalysts under both CO and CO_2 hydrogenation reactions was observed, in which the spent catalysts after CO_2 hydrogenation [sCZA-L(CO_2) and sCZA-H(CO_2)] presented large amounts of carbon deposition when compared to those after CO hydrogenation [sCZA-L(CO) and sCZA-H(CO)]. This is probably due to CO_2 hydrogenation producing more CO and H_2O [reverse water-gas-shift (RWGS)], which deactivates the catalysts.[53] It was widely reported that water is a byproduct in RWGS, which limits the

https://doi.org/10.1021/acsomega.2c03068
ACS Omega 2022, 7, 25783−25797

Scheme 1. Conceptual Model of the Structural Metal Behavior of CZA Catalysts during CO and CO_2 Hydrogenation under Atmospheric Pressure at 250 °C

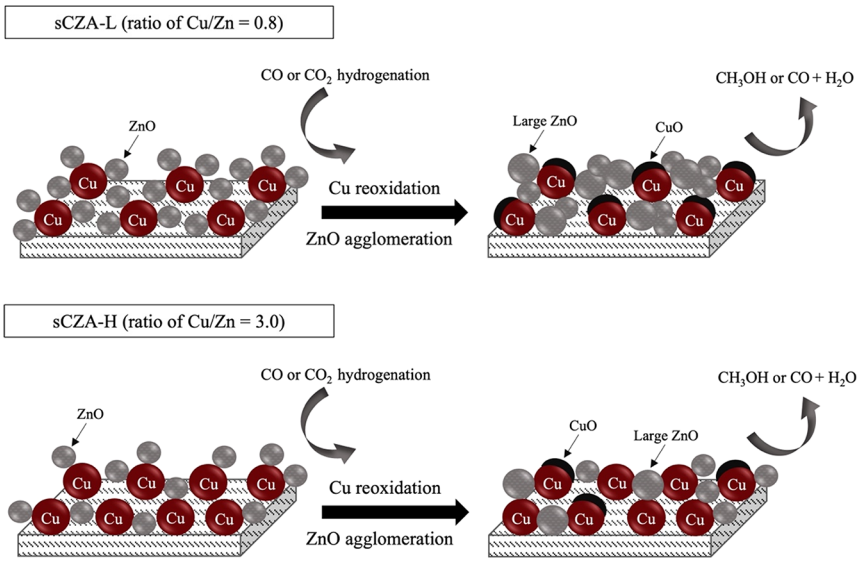

thermodynamically reaction system and affects the catalyst deactivation on active sites. However, the coke deposition on the CZA-H catalyst in CO and CO_2 hydrogenation was insignificantly different. Therefore, this observation can explain the similar results obtained from different techniques (TPO, SEM−EDX, and TGA). It indicated that fast deactivation occurred on the low Cu content (high Zn content) in CZA catalysts because of low oxidation of carbonaceous materials on the catalyst surface.[52,54]

3.3. Possible Deactivation Cause in This Study. Based on the above observations, the main cause of the catalyst deterioration observed in the early stages of the reaction is not only the coking, but there are still also some consequences of the metal crystallite size aggregation and the unstable Cu^0 site and the increase in ZnO crystallite size. All changes in the surface of CZA catalysts after being used in CO and CO_2 hydrogenation led to the loss of active surface sites. Therefore, the deterioration of catalysts was investigated, especially the ensembles of large ZnO particles that are reported to have more impact on the coke accumulation.[14,28,51] For deep investigation on the change in the surface properties for spent catalysts, it shows that the activity and stability are essentially related to the size and amount of the ZnO particles and the carbon deposition. According to these results, catalysts with large and/or high amount of ZnO particles are not only hardly active for the decreased CO and CO_2 conversion (as seen in Table 1), but they also tend to deactivate rapidly since the coke formation is enhanced. In our view, the catalyst having high amounts of ZnO in the CZA catalyst showed decreased catalytic activity and increased coking after hydrogenation reactions for both CO and CO_2. This is in good agreement with all characteristic results, indicating the lesser stabilizing surface and larger particle sizes by metal aggregation. Possible models of the metal aggregation by crystallite growth after CO and CO_2 hydrogenation over CZA-L and CZA-H catalysts are illustrated in Scheme 1. The metal aggregation mechanism is known as metal sintering, which resulted in the reduction of the surface area and loss of active sites by increasing the metal crystallite size.[55] This results in a decrease in catalytic activity, and it is the cause of the deactivation of metal catalysts. Therefore, the more stable Cu site on surface catalysts is obtained from lower ZnO contents (CZA-H) associated with a high Cu dispersion and a strong textural growth of Cu^0 metal particle sites, resulting in a higher catalytic activity and stability of CZA catalysts. This is because a high ZnO content may be agglomerated, causing the loss of Cu active sites. A large amount of research has been conducted to overcome the imperfection of Cu/ZnO catalysts in hydrogenation. The authors found that the addition of appropriate amounts of ZnO content is beneficial for preventing of Cu particle agglomeration and supporting the synergistic effect of the Cu-ZnO interface. Furthermore, the effect of the loss of Cu active sites and ZnO agglomeration can be improved by the addition suitable promoters (metal oxides such as Al_2O_3, Cr_3O_3, MgO, ZrO_2, CeO_2, and MnO_2) to inhibit the Cu^{2+} reduction to inactive and stabilized Cu species and to stabilize the ZnO species,[28,35] respectively. In addition, the regeneration process of Cu-based catalysts is related to the ability of Cu reduction and Cu oxidation; therefore, some metal species (Cr and Mg) can promote the large Cu surface area and improve Cu distribution. This is beneficial to resist the metal sintering of catalysts. Additionally, coke formation is normally the main reason for deactivation in solid catalysts depending on the catalytic properties of active metal sites and the reaction condition.[14,28] This is because of the different reaction pathways over the base metal and the nature of the catalyst support. The understanding of carbon deposition (coke) is important for the development of metal-based catalysts used in the chemical industry with high catalytic performance (activity and stability). According to several research studies, the possible coke formation can be classified into three categories.[14,55] First, carbon (or coke) is chemically and/or physically adsorbed as a monolayer (carbide formation) and/or multilayer, respectively. In this case, it will block the accessibility of reactants to metallic sites. Second, the carbon deposition will cover the metal surface (carbon encapsulation), leading to deactivation of the active sites. Third, the carbon is formed in the pores of the catalyst, and then the active sites or pores are blocked, resulting in the loss of the accessible reactant opportunity. Therefore, the important factor of coke

https://doi.org/10.1021/acsomega.2c03068
ACS Omega 2022, 7, 25783−25797

Scheme 2. Conceptual Model of the Coke Deposition over CZA Catalysts during CO and CO_2 Hydrogenation under Atmospheric Pressure at 250 °C

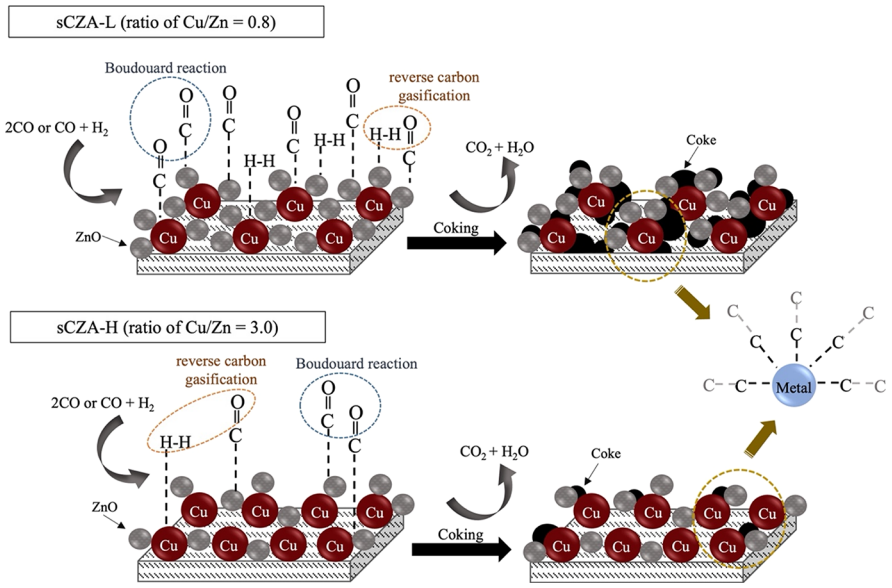

deposition on the catalyst surface depends on the catalyst structure including the interaction between the metal and support, metal particle size, or the crystallite size of metal that result in promotion of coke formation. In our previous work, we explained the formation of coke on the catalyst surface in the last part for the elementary in some reason of catalytic deactivation by coke formation. It can be proven by more results in the above section of structural characterization for the identified coke. These results also confirmed the decrease in the catalytic activity by the coke formation. Due to the complexity of the coke feature, the conceptual model of carbon deposition (coke) on the catalyst surface is depicted in Scheme 2. The formation of coke takes place together with the first step of methanol synthesis from the pathway of its intermediates (formate, carboxyl, and formyl species) via CO and CO_2 hydrogenation, and after that, coke is generated in this reaction. These results may suggest that the carbon formation as a filament or amorphous coke on surface catalysts occurs via the Boudouard reaction (or CO disproportionation, eq 6) to desorb CO_2 molecules without hydrogen consumption at low temperatures.[16,55] Additionally, another possible pathway for carbon formation is a CO reduction (or reverse carbon gasification, eq 7), in which CO is reduced by H_2 molecules to release water and is favorable at low temperatures. The residue of carbon will diffuse through metal, and after that, the chemisorption of metal carbide is generated over metal sites, resulting in a carbon atom in close contact with other carbon atoms that are necessary to aggregate the larger size of carbon deposition in both of physisorption (C−C, surface carbide) and chemisorption (metal carbide).[14,49] The carbon accumulation (coke) covered on Cu in the metallic function and partially blocked metal interface interaction of Cu-ZnO sites plays a significant role in the performance of active sites. These effects resulted in the decreased chance of product formation (the activity of catalyst) as a function of time. Moreover, these results are confirmed by surface characterizations such as SEM−EDX, BET, and TPO analysis, which identified the surface structure with carbon deposition. It is evident that the different amounts of ZnO content in the metal surface catalyst resulted in the deactivated catalysts (catalyst lifetime) together with the large size of ZnO particles that is more pronounced for catalytic deactivation. According to the relevance of catalyst deactivation by coke deposition, it showed more carbon accumulation on the metal surface with increasing the ZnO content in catalysts, leading to accelerate the catalyst deterioration.

However, this finding may depend on the feed composition because some researchers discovered that in methanol synthesis by the hydrogenation reaction, the coke deposition is more pronounced using only pure CO or CO_2 in feed. However, the coke formation on the metal surface of the Cu/ZnO/Al_2O_3 catalyst is less formed with cofeeding of CO and CO_2 (CO/CO_2 hydrogenation) because the carbon oxidation during the reaction can occur.[56] The adding of CO_2 as a mixing feed for CO hydrogenation can prevent the deactivation of the active catalyst surface (Cu-based) and maintain the active surface site, whereas CO and H_2 in the reaction mixture support the opportunity to form an inactive Cu site.[28,29,57] As mentioned above, Cu/ZnO-based catalysts have a specific hydrogenation reaction (CO and CO_2) activity and stability under mild conditions. Therefore, it is a promising catalyst for industrial application.

4. CONCLUSIONS

The ternary Cu/ZnO/Al_2O_3 (CZA) catalysts having different Cu contents were synthesized by the coprecipitation method and were tested in CO and CO_2 hydrogenation. It was found that the amount of Cu active sites affected the catalytic activity. The conversion of CO and CO_2 in hydrogenation decreased with increasing amounts of ZnO (Cu:Zn of 0.8). Moreover, the low amount of Cu content in CZA-L showed a low catalytic activity. Therefore, the CZA-L exhibited a faster deactivation than CZA-H for both CO and CO_2 hydrogenation. In addition, the physicochemical properties of fresh and spent catalysts were determined to further explain the deactivation behaviors of the CZA catalysts in these reactions. The major cause of catalyst deactivation is attributed to the changes in the arrangement of metal sites, structure of CZA

https://doi.org/10.1021/acsomega.2c03068
ACS Omega 2022, 7, 25783−25797

catalysts, and the carbon deposition during the reaction test. This can be concluded that the high aggregation of Cu, ZnO crystallite size, and the high amount of coke formation in CZA-L after hydrogenation of CO and CO_2 [sCZA-L(CO) and sCZA-L(CO_2)] led to a decrease in catalytic activity due to catalyst deactivation, whereas the opposite phenomena were evident for the CZA-H catalyst.

■ ASSOCIATED CONTENT

Supporting Information

The Supporting Information is available free of charge at https://pubs.acs.org/doi/10.1021/acsomega.2c03068.

Schematic illustration of a continuous fixed-bed reactor for CO and CO_2 hydrogenation, elemental mapping of the fresh CZA-L catalyst, elemental mapping of the sCZA-L(CO) catalyst, elemental mapping of the sCZA-L(CO_2) catalyst, elemental mapping of the fresh CZA-H catalyst, elemental mapping of the sCZA-H(CO) catalyst, and elemental mapping of sCZA-H(CO_2) catalyst (PDF)

■ AUTHOR INFORMATION

Corresponding Author

Bunjerd Jongsomjit − *Center of Excellence on Catalysis and Catalytic Reaction Engineering (CECC), Department of Chemical Engineering, Faculty of Engineering, Chulalongkorn University, Bangkok 10330, Thailand;* orcid.org/0000-0002-9558-9190; Phone: +66-221-86874; Email: bunjerd.j@chula.ac.th; Fax: +66-221-86877

Authors

Tanutporn Kamsuwan − *Center of Excellence on Catalysis and Catalytic Reaction Engineering (CECC), Department of Chemical Engineering, Faculty of Engineering, Chulalongkorn University, Bangkok 10330, Thailand*

Adisak Guntida − *Center of Excellence on Catalysis and Catalytic Reaction Engineering (CECC), Department of Chemical Engineering, Faculty of Engineering, Chulalongkorn University, Bangkok 10330, Thailand*

Piyasan Praserthdam − *Center of Excellence on Catalysis and Catalytic Reaction Engineering (CECC), Department of Chemical Engineering, Faculty of Engineering, Chulalongkorn University, Bangkok 10330, Thailand;* orcid.org/0000-0001-8021-2115

Complete contact information is available at: https://pubs.acs.org/10.1021/acsomega.2c03068

Notes

The authors declare no competing financial interest.

■ ACKNOWLEDGMENTS

This research is supported by Ratchadapisek Somphot Fund for Postdoctoral Fellowship, Chulalongkorn University. The authors also would like to acknowledge Chulalongkorn University (under the Ratchadapisek Somphot and Fundamental Fund) and Malaysia-Thailand Joint Authority (MTJA) for supporting this research.

■ REFERENCES

(1) Dasireddy, V. D. B. C.; Likozar, B. The role of copper oxidation state in Cu/ZnO/Al_2O3 catalysts in CO_2 hydrogenation and methanol productivity. *Renewable Energy* **2019**, *140*, 452−460.

(2) Gogate, M. R. Methanol synthesis revisited: reaction mechanisms in CO/CO_2 hydrogenation over Cu/ZnO and DFT analysis. *Pet. Sci. Technol.* **2019**, *37*, 603−610.

(3) Kamsuwan, T.; Krutpijit, C.; Praserthdam, S.; Phatanasri, S.; Jongsomjit, B.; Praserthdam, P. Comparative study on the effect of different copper loading on catalytic behaviors and activity of Cu/ZnO/Al_2O_3 catalysts toward CO and CO_2 hydrogenation. *Heliyon* **2021**, *7*, No. e07682.

(4) Bowker, M. Methanol Synthesis from CO_2 Hydrogenation. *ChemCatChem* **2019**, *11*, 4238−4246.

(5) Sadeghinia, M.; Rezaei, M.; Nemati Kharat, A.; Namayandeh Jorabchi, M.; Nematollahi, B.; Zareiekordshouli, F. Effect of In_2O_3 on the structural properties and catalytic performance of the CuO/ZnO/Al_2O_3 catalyst in CO_2 and CO hydrogenation to methanol. *Mol. Catal.* **2020**, *484*, No. 110776.

(6) Vu, T. T. N.; Desgagnés, A.; Iliuta, M. C. Efficient approaches to overcome challenges in material development for conventional and intensified CO_2 catalytic hydrogenation to CO, methanol, and DME. *Appl. Catal., A* **2021**, *617*, No. 118119.

(7) Atsonios, K.; Panopoulos, K. D.; Kakaras, E. Investigation of technical and economic aspects for methanol production through CO_2 hydrogenation. *Int. J. Hydrogen Energy* **2016**, *41*, 2202−2214.

(8) Qi, T.; Zhao, Y.; Chen, S.; Li, W.; Guo, X.; Zhang, Y.; Song, C. Bimetallic metal organic framework-templated synthesis of a Cu-ZnO/Al_2O_3 catalyst with superior methanol selectivity for CO_2 hydrogenation. *Mol. Catal.* **2021**, *514*, No. 111870.

(9) Liu, Y.-M.; Liu, J.-T.; Liu, S.-Z.; Li, J.; Gao, Z.-H.; Zuo, Z.-J.; Huang, W. Reaction mechanisms of methanol synthesis from CO/CO_2 hydrogenation on Cu_2O(111): Comparison with Cu(111). *J. CO2 Util.* **2017**, *20*, 59−65.

(10) Zhang, L.-x.; Zhang, Y.-c.; Chen, S.-y. Effect of promoter TiO_2 on the performance of CuO-ZnO-Al_2O_3 catalyst for CO_2 catalytic hydrogenation to methanol. *J. Fuel Chem. Technol.* **2011**, *39*, 912−917.

(11) Ren, H.; Xu, C.-H.; Zhao, H.-Y.; Wang, Y.-X.; Liu, J.; Liu, J.-Y. Methanol synthesis from CO_2 hydrogenation over Cu/γ-Al_2O_3 catalysts modified by ZnO, ZrO_2 and MgO. *J. Ind. Eng. Chem.* **2015**, *28*, 261−267.

(12) Chiang, C.-L.; Lin, K.-S.; Chuang, H.-W. Direct synthesis of formic acid via CO_2 hydrogenation over Cu/ZnO/Al_2O_3 catalyst. *J. Cleaner Prod.* **2018**, *172*, 1957−1977.

(13) Chu, Z.; Chen, H.; Yu, Y.; Wang, Q.; Fang, D. Surfactant-assisted preparation of Cu/ZnO/Al_2O_3 catalyst for methanol synthesis from syngas. *J. Mol. Catal. A: Chem.* **2013**, *366*, 48−53.

(14) Argyle, M.; Bartholomew, C. Heterogeneous Catalyst Deactivation and Regeneration: *A Review*. *Catalysts* **2015**, *5*, 145.

(15) Fichtl, M. B.; Schlereth, D.; Jacobsen, N.; Kasatkin, I.; Schumann, J.; Behrens, M.; Schlögl, R.; Hinrichsen, O. Kinetics of deactivation on Cu/ZnO/Al_2O_3 methanol synthesis catalysts. *Appl. Catal., A* **2015**, *502*, 262−270.

(16) Wittich, K.; Krämer, M.; Bottke, N.; Schunk, S. A. Catalytic Dry Reforming of Methane: Insights from Model Systems. *ChemCatChem* **2020**, *12*, 2130.

(17) Allam, D.; Cheknoun, S.; Hocine, S. Operating Conditions and Composition Effect on the Hydrogenation of Carbon Dioxide Performed over CuO/ZnO/Al_2O_3 Catalysts. *Bull. Chem. React. Eng. Catal.* **2019**, *14*, 604−613.

(18) Bali, F.; Jalowiecki-Duhamel, L. CO_2 Hydrogenation to Methanol on Cu−ZrO_2 Catalysts. In *Global Warming: Engineering Solutions*, Dincer, I.; Hepbasli, A.; Midilli, A.; Karakoc, T. H. Eds.; Springer US, 2010; pp. 315−327, DOI: 10.1007/978-1-4419-1017-2_19.

(19) Peláez, R.; Bryce, E.; Marín, P.; Ordóñez, S. Catalyst deactivation in the direct synthesis of dimethyl ether from syngas over CuO/ZnO/Al_2O_3 and γ-Al_2O_3 mechanical mixtures. *Fuel Process. Technol.* **2018**, *179*, 378−386.

(20) Bozzano, G.; Manenti, F. Efficient methanol synthesis: Perspectives, technologies and optimization strategies. *Prog. Energy Combust. Sci.* **2016**, *56*, 71−105.

(21) Fang, X.; Men, Y.; Wu, F.; Zhao, Q.; Singh, R.; Xiao, P.; Du, T.; Webley, P. A. Moderate-pressure conversion of H_2 and CO_2 to methanol via adsorption enhanced hydrogenation. *Int. J. Hydrogen Energy* **2019**, *44*, 21913−21925.
(22) Cai, X.; Ke, Y.; Wang, B.; Zeng, Y.; Chen, L.; Li, Y.; Bai, G.; Yan, X. Efficient catalytic amination of diols to diamines over Cu/ZnO/γ-Al_2O_3. *Mol. Catal.* **2021**, *508*, No. 111608.
(23) Panyad, S.; Jongpatiwut, S.; Sreethawong, T.; Rirksomboon, T.; Osuwan, S. Catalytic dehydroxylation of glycerol to propylene glycol over Cu−ZnO/Al_2O_3 catalysts: Effects of catalyst preparation and deactivation. *Catal. Today* **2011**, *174*, 59−64.
(24) Hu, X.; Qin, W.; Guan, Q.; Li, W. The Synergistic Effect of $CuZnCeO_x$ in Controlling the Formation of Methanol and CO from CO_2 Hydrogenation. *ChemCatChem* **2018**, *10*, 4438−4449.
(25) Li, S.; Guo, L.; Ishihara, T. Hydrogenation of CO_2 to methanol over Cu/AlCeO catalyst. *Catal. Today* **2020**, *339*, 352−361.
(26) Pasupulety, N.; Driss, H.; Alhamed, Y. A.; Alzahrani, A. A.; Daous, M. A.; Petrov, L. Studies on Au/Cu−Zn−Al catalyst for methanol synthesis from CO_2. *Appl. Catal., A* **2015**, *504*, 308−318.
(27) Zhan, H.; Shi, X.; Tang, B.; Wang, G.; Ma, B.; Liu, W. The performance of Cu/Zn/Zr catalysts of different Zr/(Cu+Zn) ratio for CO_2 hydrogenation to methanol. *Catal. Commun.* **2021**, *149*, No. 106264.
(28) Ay, S.; Ozdemir, M.; Melikoglu, M. Effects of metal promotion on the performance, catalytic activity, selectivity and deactivation rates of Cu/ZnO/Al_2O_3 catalysts for methanol synthesis. *Chem. Eng. Res. Des.* **2021**, *175*, 146−160.
(29) Dalebout, R.; Visser, N. L.; Pompe, C. E. L.; de Jong, K. P.; de Jongh, P. E. Interplay between carbon dioxide enrichment and zinc oxide promotion of copper catalysts in methanol synthesis. *J. Catal.* **2020**, *392*, 150−158.
(30) Zuo, Z.-J.; Wang, L.; Han, P.-D.; Huang, W. Methanol synthesis by CO and CO2 hydrogenation on Cu/γ-Al_2O_3 surface in liquid paraffin solution. *Appl. Surf. Sci.* **2014**, *290*, 398−404.
(31) Ahmad, R.; Hellinger, M.; Buchholz, M.; Sezen, H.; Gharnati, L.; Wöll, C.; Sauer, J.; Döring, M.; Grunwaldt, J.-D.; Arnold, U. Flame-made Cu/ZnO/Al_2O_3 catalyst for dimethyl ether production. *Catal. Commun.* **2014**, *43*, 52−56.
(32) Li, M.; Jiao, L.; Nawaz, M. A.; Cheng, L.; Meng, C.; Yang, T.; Tariq, M.; Liu, D. A one-step synthesis method of durene directly from syngas using integrated catalyst of Cu/ZnO/Al_2O_3 and Co-Nb/HZSM-5. *Chem. Eng. Sci.* **2019**, *200*, 103−112.
(33) Sharma, S. K.; Khan, T. S.; Singha, R. K.; Paul, B.; Poddar, M. K.; Sasaki, T.; Bordoloi, A.; Samanta, C.; Gupta, S.; Bal, R. Design of highly stable MgO promoted Cu/ZnO catalyst for clean methanol production through selective hydrogenation of CO_2. *Appl. Catal., A* **2021**, *623*, No. 118239.
(34) Si, C.; Ban, H.; Chen, K.; Wang, X.; Cao, R.; Yi, Q.; Qin, Z.; Shi, L.; Li, Z.; Cai, W.; Li, C. Insight into the positive effect of Cu^0/Cu^+ ratio on the stability of Cu-ZnO-CeO_2 catalyst for syngas hydrogenation. *Appl. Catal., A* **2020**, *594*, No. 117466.
(35) Qi, T.; Li, W.; Li, H.; Ji, K.; Chen, S.; Zhang, Y. Yttria-doped Cu/ZnO catalyst with excellent performance for CO_2 hydrogenation to methanol. *Mol. Catal.* **2021**, *509*, No. 111641.
(36) Mousavi-Kamazani, M. Facile sonochemical-assisted synthesis of Cu/ZnO/Al_2O_3 nanocomposites under vacuum: Optical and photocatalytic studies. *Ultrason. Sonochem.* **2019**, *58*, No. 104636.
(37) Fu, L.; Li, X.; Liu, M.; Yang, H. Insights into the nature of Cu doping in amorphous mesoporous alumina. *J. Mater. Chem. A* **2013**, *1*, 14592−14605.
(38) Li, L.; Hu, C.; Zhang, L.; Shi, B. More octahedral Cu^+ and surface acid sites in uniformly porous Cu-Al_2O_3 for enhanced Fenton catalytic performances. *J. Hazard. Mater.* **2021**, *406*, No. 124739.
(39) Liao, M.; Qin, H.; Guo, W.; Gao, P.; Xiao, H. Porous reticular CuO/ZnO/CeO_2/ZrO_2 catalyst derived from polyacrylic acid hydrogel system on Al_2O_3 foam ceramic support for methanol steam reforming microreactor. *Ceram. Int.* **2021**, *47*, 33667−33677.
(40) Tong, R.; Fu, R.; Yang, Z.; Jiang, Y.; Jiang, K.; Sun, X. Efficient degradation of sulfachloropyridazine by sulfite activation with CuO-Al_2O_3 composites under neutral pH conditions: Radical and non-radical. *J. Environ. Chem Eng.* **2022**, *10*, No. 107276.
(41) Ai, X.; Xie, H.; Chen, S.; Zhang, G.; Xu, B.; Zhou, G. Highly dispersed mesoporous Cu/γ-Al_2O_3 catalyst for RWGS reaction. *Int. J. Hydrogen Energy* **2022**, *47*, 14884−14895.
(42) Qi, S.-C.; Liu, X.-Y.; Zhu, R.-R.; Xue, D.-M.; Liu, X.-Q.; Sun, L.-B. Causation of catalytic activity of Cu-ZnO for CO_2 hydrogenation to methanol. *Chem. Eng. J.* **2022**, *430*, No. 132784.
(43) Zhang, F.; Liu, Y.; Xu, X.; Yang, P.; Miao, P.; Zhang, Y.; Sun, Q. Effect of Al-containing precursors on Cu/ZnO/Al_2O_3 catalyst for methanol production. *Fuel Process. Technol.* **2018**, *178*, 148−155.
(44) Hua, Y.; Guo, X.; Mao, D.; Lu, G.; Rempel, G. L.; Ng, F. T. T. Single-step synthesis of dimethyl ether from biomass-derived syngas over CuO-ZnO-MO_x (M=Zr, Al, Cr, Ti)/HZSM-5 hybrid catalyst: Effects of MOx. *Appl. Catal., A* **2017**, *540*, 68−74.
(45) Liu, C.; Guo, X.; Guo, Q.; Mao, D.; Yu, J.; Lu, G. Methanol synthesis from CO2 hydrogenation over copper catalysts supported on MgO-modified TiO_2. *J. Mol. Catal. A: Chem.* **2016**, *425*, 86−93.
(46) Liang, B.; Ma, J.; Su, X.; Yang, C.; Duan, H.; Zhou, H.; Deng, S.; Li, L.; Huang, Y. Investigation on Deactivation of Cu/ZnO/Al_2O_3 Catalyst for CO_2 Hydrogenation to Methanol. *Ind. Eng. Chem. Res.* **2019**, *58*, 9030−9037.
(47) Arena, F.; Barbera, K.; Italiano, G.; Bonura, G.; Spadaro, L.; Frusteri, F. Synthesis, characterization and activity pattern of Cu−ZnO/ZrO_2 catalysts in the hydrogenation of carbon dioxide to methanol. *J. Catal.* **2007**, *249*, 185−194.
(48) Dasireddy, V. D. B. C.; Neja, S. Š.; Blaž, L. Correlation between synthesis pH, structure and Cu/MgO/Al_2O_3 heterogeneous catalyst activity and selectivity in CO_2 hydrogenation to methanol. *J. CO2 Util.* **2018**, *28*, 189−199.
(49) Zhuang, Y.; Currie, R.; McAuley, K. B.; Simakov, D. S. A. Highly-selective CO_2 conversion via reverse water gas shift reaction over the 0.5wt% Ru-promoted Cu/ZnO/Al_2O_3 catalyst. *Appl. Catal., A* **2019**, *575*, 74−86.
(50) Ren, S.; Fan, X.; Shang, Z.; Shoemaker, W. R.; Ma, L.; Wu, T.; Li, S.; Klinghoffer, N. B.; Yu, M.; Liang, X. Enhanced catalytic performance of Zr modified CuO/ZnO/Al_2O_3 catalyst for methanol and DME synthesis via CO_2 hydrogenation. *J. CO2 Util.* **2020**, *36*, 82−95.
(51) Gayubo, A. G.; Vicente, J.; Ereña, J.; Oar-Arteta, L.; Azkoiti, M. J.; Olazar, M.; Bilbao, J. Causes of deactivation of bifunctional catalysts made up of CuO-ZnO-Al_2O_3 and desilicated HZSM-5 zeolite in DME steam reforming. *Appl. Catal., A* **2014**, *483*, 76−84.
(52) Wu, Q.; To, A. T.; Nash, C. P.; Dupuis, D. P.; Baddour, F. G.; Habas, S. E.; Ruddy, D. A. Spectroscopic insight into carbon speciation and removal on a Cu/BEA catalyst during renewable high-octane hydrocarbon synthesis. *Appl. Catal., B* **2021**, *287*, No. 119925.
(53) Guil-López, R.; Mota, N.; Llorente, J.; Millán, E.; Pawelec, B.; Fierro, J. L. G.; Navarro, R. M. Methanol Synthesis from CO_2: A Review of the Latest Developments in Heterogeneous Catalysis. *Materials* **2019**, *12*, 3902.
(54) Pampararo, G.; Garbarino, G.; Riani, P.; Villa García, M.; Sánchez Escribano, V.; Busca, G. A study of ethanol dehydrogenation to acetaldehyde over supported copper catalysts: Catalytic activity, deactivation and regeneration. *Appl. Catal., A* **2020**, *602*, No. 117710.
(55) Ochoa, A.; Bilbao, J.; Gayubo, A. G.; Castaño, P. Coke formation and deactivation during catalytic reforming of biomass and waste pyrolysis products: A review. *Renewable Sustainable Energy Rev.* **2020**, *119*, No. 109600.
(56) Prašnikar, A.; Dasireddy, V. D. B. C.; Likozar, B. Scalable combustion synthesis of copper-based perovskite catalysts for CO_2 reduction to methanol: Reaction structure-activity relationships, kinetics, and stability. *Chem. Eng. Sci.* **2022**, *250*, No. 117423.
(57) Song, H.-t.; Fazeli, A.; Kim, H. D.; Alizadeh Eslami, A.; Noh, Y. S.; Ghaffari Saeidabad, N.; Moon, D. J. Effect of lanthanum group promoters on Cu/(mixture of ZnO and Zn-Al-spinnel-oxides) catalyst for methanol synthesis by hydrogenation of CO and CO_2 mixtures. *Fuel* **2021**, *283*, No. 118987.

https://doi.org/10.1021/acsomega.2c03068
ACS Omega 2022, 7, 25783−25797